The effect of membrane thickness on AEMFC Performance: An integrated theoretical and experimental study

Karam Yassin, John Douglin, Igal Rasin, Pietro Santori, Björn Eriksson, Nicolas Bibent, Frédéric Jaouen, Simon Brandon, Dario Dekel

▶ **To cite this version:**

Karam Yassin, John Douglin, Igal Rasin, Pietro Santori, Björn Eriksson, et al.. The effect of membrane thickness on AEMFC Performance: An integrated theoretical and experimental study. Energy Conversion and Management, 2023, 270, pp.116203. 10.1016/j.enconman.2022.116203 . hal-03859978

HAL Id: hal-03859978

https://hal.umontpellier.fr/hal-03859978v1

Submitted on 19 Oct 2023

HAL is a multi-disciplinary open access archive for the deposit and dissemination of scientific research documents, whether they are published or not. The documents may come from teaching and research institutions in France or abroad, or from public or private research centers.

L'archive ouverte pluridisciplinaire **HAL**, est destinée au dépôt et à la diffusion de documents scientifiques de niveau recherche, publiés ou non, émanant des établissements d'enseignement et de recherche français ou étrangers, des laboratoires publics ou privés.

The Effect of Membrane Thickness on AEMFC Performance: An Integrated Theoretical and Experimental Study

Karam Yassin [a], John C. Douglin [a], Igal G. Rasin [a], Pietro G. Santori [b], Björn Eriksson [b], Nicolas Bibent[b], Frédéric Jaouen [b], Simon Brandon [a,c,] and Dario R. Dekel [a,c,*]*

[a] The Wolfson Department of Chemical Engineering, Technion – Israel Institute of Technology, Haifa 3200003, Israel

[b] ICGM, Univ. Montpellier, CNRS, ENSCM, Montpellier, France

[c] The Nancy & Stephen Grand Technion Energy Program (GTEP), Technion – Israel Institute of Technology, Haifa 3200003, Israel

* Corresponding authors

E-mail addresses: dario@technion.ac.il (D.R. Dekel), cersbsb@technion.ac.il (S. Brandon)

Highlights

- The critical effect of AEM thickness on AEMFC performance was investigated
- Reduced membrane thickness significantly enhances AEMFC performance
- Good agreement between model simulations and experimental results were obtained
- Anode flooding and cathode dehydration can be suppressed by using thin AEM
- AEM thickness has a strong impact on cathode hydration levels and ORR kinetics

Abstract

We present a comprehensive theoretical and experimental study of the effect of membrane thickness on the anion-exchange membrane (AEM) fuel cell (AEMFC) performance. AEMFC tests are carried out with several AEMs with thickness in the range of 5 – 50 μm and assembled with a PtRu anode, and two different cathode catalysts (Pt/C or Fe-N-C). Dramatic improvements in cell performance are observed as the membrane thickness decreases, which is mainly attributed to reduced ohmic losses and enhanced water transport between the electrodes. The simulated cell performance obtained using our previously developed AEMFC model qualitatively and quantitatively explains the experimental results in the entire range of current densities (0-4 Acm^{-2}). Simulated results show that thinner membranes enhance water transport between the electrodes, mitigating the anode flooding, and resulting in increased local hydration in the membrane and cathode catalytic layer. These high hydration values enhance the anionic conductivity of the ionomeric materials, thereby improving cell performance. Furthermore, the enhanced water transport towards the cathode electrode provides sufficient water to participate in the oxygen reduction reaction, thus reducing the activation losses. Simulation modeling allows for a thorough understanding of cell behavior and aids in the development of the next generation of advanced AEMFCs.

Keywords: Anion-exchange membrane; Anion-exchange membrane fuel cell; Water management; Modeling; Anode flooding; Cell performance.

Graphical abstract

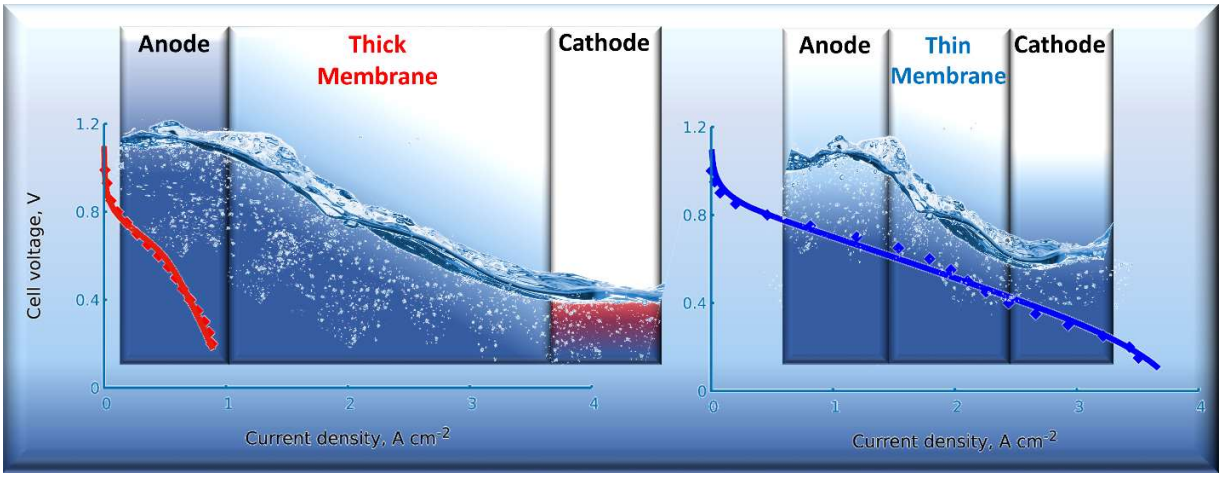

1. Introduction

Over the last decade, considerable advances have been made in the development of high-performance anion-exchange membrane fuel cells (AEMFCs) [1–3]. Affordable and abundant platinum group metal (PGM)-free catalysts for both the anode and cathode are being developed and integrated into the electrodes and cells, with promising results towards high-performance and PGM-free AEMFCs [4–16]. In addition, an extensive variety of cost-effective anion exchange membranes (AEMs) have been synthesized and implemented in AEMFCs, demonstrating outstanding performance, competitive with the state-of-the-art of proton-exchange membrane fuel cells (PEMFCs) [17–28].

However, despite the encouraging progress in AEMFC performance, water management in the system remains a significant challenge for developing this technology [29–36]. During cell operation, specifically at high current density, deficient water supply and excessive water consumption severely reduce hydration levels at the cathode side [37]. Low hydration values decrease the hydroxide conductivity within the ionomeric materials of the membrane (near the cathode side) and the cathode catalytic layer (CL). This, in turn, causes higher ohmic losses in

some regions of the membrane and in the cathode CL, which reduces cell performance [37]. Similarly, anode over-hydration and poor water removal may cause anode flooding, negatively affecting cell performance [29,33,36]. Thus, to maximize AEMFC performance, a delicate water balance between the anode and cathode is necessary. While several strategies have been proposed to mitigate the simultaneous anode flooding and cathode drying [35], high AEMFC performance has mainly been achieved with the use of thinner AEMs, in the range of 5 – 25 μm [27,38,39].

The thickness of the AEM is indeed critical in determining the flux of water diffusing from anode to cathode during operation and thus critical in the distribution of water hydration levels perpendicular to the AEM plane. This directly affects the local anionic conductivity of the ionomeric materials (especially on or near the cathode side) and, thus, also the overall cell ohmic resistance. When a thinner AEM is used, greater water back-diffusion through the membrane is achieved, resulting in a more even through-plane water distribution (for otherwise unchanged conditions, such as a MEA, operating conditions, and current density) [40]. This decreases the tendency of the anode flooding, alleviates cathode catalyst layer dry-out, and also increases the hydration in the membrane locally on or near the cathode [41][22]. Despite the importance of AEM thickness on water management and, as a result, on AEMFC performance, limited studies have been dedicated to systematically investigate this effect on AEMFC behavior [22].

Modeling AEMFC performance has proven to be a critical tool for investigating and understanding the effect of design and operating parameters on the water and hydroxide transport across the cell [31,32,34,42–47]. Generally, numerical models are validated by comparing the computed initial cell performance with the measured polarization curve. However, two or more polarization curves that are in good agreement with experimental data are required to predict cell performance accurately [48]. In this study, we measure the performance of AEMFCs assembled with FAA-3

AEMs of different thicknesses, namely 5, 10, 20, 30, or 50 μm. Next, in order to quantitatively analyze the influence of these parameters on cell performance, we apply our AEMFC comprehensive model described in [42]. First, we show the comparison of six calculated polarization curves against the experimental data. Then, we discuss the effect of AEM thickness on hydration levels, ohmic resistance, water flux, and reactions distribution across the cell. Finally, we summarize the key findings and provide a guidelines for the next generation of AEM design for fuel cell technology.

2. Experimental

2.1 Catalyst, Electrode, and Ionomeric Materials

The electrode preparation and fuel cell testing were carried out at Technion for the measurements with Pt/C cathode, and at ICGM for measurements with the Fe-N-C cathode, with a generally similar procedure. The description is detailed separately below and in section 2.2 for these two measurement sets.

For the cells comprising a Pt/C cathode, PtRu/C anode catalyst (40% Pt and 20% Ru on carbon black, HiSPEC® 10000, with 2:1 Pt:Ru mass ratio supported on Vulcan XC 72R) and Pt/C cathode catalyst (40% Pt on carbon black, HiSPEC® 4000) were purchased from Alfa Aesar. For the cells comprising a Fe-N-C cathode, the anode catalyst was prepared from HiSPEC® 10000, by mixing it with the amount of uncatalyzed carbon black (Vulcan XC 72R) needed to decrease the PGM content to 40 wt% PtRu/C. The Fe-N-C cathode catalyst was prepared following a previously published procedure, as reported in detail in [5][49]. In brief, optimized amounts of anhydrous ferrous acetate, 1,10-phenanthroline and the metal-organic framework ZIF-8 were dry-mixed with planetary ball-milling, then pyrolyzed in flowing Ar at 1050°C, then pyrolyzed in flowing NH_3 at

950°C. This catalyst was shown by spectroscopy and microscopy to comprise Fe mainly as atomically-dispersed Fe-N_4 sites [5][49]. For electrode preparation, Toray carbon paper, TGP-H-060 with 5 wt% PTFE wet-proofing was purchased from FuelCellStore.

The AEMs used in this study lean on the FAA-3 chemistry, a commercial ionomeric material with anion-conducting properties, received from Fumatech GmbH (Germany). Five AEMs of different thicknesses were kindly provided by Fumatech in bromide form – FAA-3-05-rf, FAA-3-10, FAA-3-PE-20, FAA-3-30, and FAA-3-50. The last two digits correspond to the membrane thickness in μm. The anion-exchange ionomer used for the electrodes was a developmental material consisting of crosslinked polystyrene functionalized with trimethylamine, also supplied by Fumatech.

2.2 Membrane electrode assembly (MEA) fabrication

For the cells with a Pt/C cathode, the gas diffusion electrode method was employed to prepare the electrodes, following previously published procedures reported elsewhere [50][51]. Three pairs of anodes and cathodes gas diffusion electrodes were loaded to 0.7 ± 0.05 mg_{PtRu} cm^{-2} and 0.7 ± 0.05 mg_{Pt} cm^{-2}, respectively. Each pair of electrodes along with a 12.25 cm^2 piece of the AEM were immersed in an aqueous 1 M KOH solution for 1 h, with solution changes every 20 min, to convert it to the hydroxide form. The MEA was then assembled between two 5 cm^2 single-serpentine graphite flow field plates and the cell tightened using a 4.5 N m torque.

For the cells with PGM-free cathodes, the gas diffusion electrode method was also employed to prepare the electrodes, following previously published procedures reported elsewhere [10][52]. Three pairs of anode and cathode gas diffusion electrodes were loaded to 0.4 ± 0.02 mg_{PtRu} cm^{-2} and 0.8 ± 0.05 mg_{FeNC} cm^{-2}, respectively. Each pair of electrodes along with a 9 cm^2 piece of the AEM were immersed in an aqueous 1 M KOH solution for 1 h, with solution changes every 20 min,

to convert it to the hydroxide form. The MEA was then assembled in a 5 cm^2 single-cell fuel cell (Scribner), and the cell tightened using a 5.1 N m torque.

2.3 Anion-exchange membrane fuel cell testing

All the AEMFCs were tested in an 850E Scribner Associates Fuel Cell test station. For the cells with the Pt/C cathode, the cell temperature was 60 °C with anode and cathode dewpoints of 60 °C, with H_2 and O_2 reactant gases at flow rates of 1 slpm without back-pressurization. Polarization curves were recorded potentiostatically by scanning from open-circuit voltage to 0.15 V at a scan rate of 5 mV s^{-1} to compare the beginning-of-life performances and mitigate against any degradation-related power losses.

For the cells with the Fe-N-C cathode, the cell temperature was 60 °C with anode and cathode dewpoints of 56 and 58 °C, respectively, with H_2 and O_2 reactant gases at flow rates of 1 slpm, and 2 bar back pressure applied at the cathode and no back pressure applied at the anode. Polarization curves were recorded potentiostatically by scanning from open-circuit voltage to 0.11 V, and then back up to OCV, at a moderately fast scan rate of 10 mV s^{-1} in order to mitigate against any degradation-related power losses. Only the OCV to 0.11 V scan is presented in the figures and used to compare the beginning-of-life performances.

3. Modeling approach

A one-dimensional time-dependent and isothermal model of AEMFC operation is employed in this study [42]. A five-layers MEA comprises a membrane, anode, and cathode CLs, and anode and cathode gas diffusion layers (GDLs), are included in the computational domain. The model takes into account mass transport (gas transport through GDLs and CLs as well as liquid water)

across the MEA, electrochemical reactions (hydrogen oxidation and oxygen reduction reactions), and degradation kinetics of the ionomeric material within the membrane and the CLs. Details of the model system and equations as well as our numerical approach, which is primarily based on explicit finite differences, are fully described in [37,42]. AEM properties, design parameters, and operating conditions used for model validations are summarized in Tables 1 and 2.

Table 1. FAA-3 ionomeric materials and their properties, as used in model validations.

Property	**Value**	**Ref.**
Thickness	5-50 μm	Provided by Fumatech
Conductivity	101 mS cm^{-1}	[53]
Water diffusivity	$1.25 \cdot 10^{-11} \cdot \lambda$ m^2 s^{-1}	[54–56]
AEM ion exchange capacity	1.43 mmol g^{-1}	[53]
Ionomer ion exchange capacity	2 mmol g^{-1}	[57]
Hydration number, λ (ionomer/ air humidification equilibrium)	$\lambda = 64.60RH^3 - 104.90RH^2 + 64.35RH - 11.05$	[58]
Maximum λ, λ_{max} (corresponding to ionomer/water contact)	13	[58]

Table 2. MEA design parameters and operating conditions.

Design / operating parameter	**Value**	
	Cells with Pt/C cathode	Cells with Fe-N-C Cathode
Cell temperature	60 °C	60 °C
Anode relative humidity (RH)	100 %	83 %
Cathode RH	100 %	94 %
Anode/Cathode GDL thickness	200 μm	200 μm
Anode back pressure	No backpressure	No backpressure
Cathode back pressure	No backpressure	2 bars
Polarization scan rate	5 mV s^{-1}	10 mV s^{-1}
Anode catalyst loading	0.7 mg_{PtRu} cm^{-2}	0.4 mg_{PtRu} cm^{-2}
Cathode catalyst loading	0.7 mg_{Pt} cm^{-2}	0.8 $mg_{Fe\text{-}N\text{-}C}$ cm^{-2}
Anode ionomer:carbon mass ratio	0.4	0.4
Cathode ionomer:carbon mass ratio	0.4	0.2

Cathode electrochemical surface area (fitted parameter)	410 m^2 g^{-1}	450 m^2 g^{-1}

Table . 3 Main model equations and parameters

Parameter	Value/expression	Note	Ref.
Fickian diffusion coefficient of free water	$\overline{D}_w = \tau^{-2}\left(\frac{1-x_w}{D_{wOH^-}} + \frac{1}{D_{wM}}\right)^{-1}$	Water transport in the ionomeric phase. D_{wM} - diffusion coefficient of water in AEM x_w – water mole fraction in ionomer phase - diffusion coefficient of water in AEM. D_{wOH^-} Pair diffusion coefficient, equal to $6x10^{-9}$ m^2/s τ- tortuosity	[37]
Water diffusivity in ionomer, D_{wM}	$D_{wM}(OH^-, \lambda, T) = 1.2 \cdot 10^{-11}\lambda x Exp\{1.3x10^{-10}[c_{OH^-}(- c_{OH^-}(0)]\} x Exp\left\{-\frac{E_a}{R}x\left(\frac{1}{T} - \frac{1}{333}\right)\right\}$	Function of λ, T, and IEC (equal to c_{OH^-}). T = 60 °C. c_{OH^-} Hydroxide concentration – mole/liter.	[42,43, 59]

Hydroxide diffusion in ionomer, $D_{OH^-}(t)$	$D_{OH^-}(t) = D_{OH^-}(0) \cdot \frac{c_{OH^-}(t)^2}{c_{OH^-(0)}{}^2} \cdot Exp\{1.3x10^{-10}[c_{OH^-}(t) - c_{OH^-}(0)]\}$	Local hydroxide ion diffusion in ionomer as a function of IEC (equal to c_{OH^-}).	[42]
Hydroxide conductivity in ionomer, $\sigma(c_{OH^-}, \lambda)$	$\sigma(c_{OH^-}, \lambda) = \frac{F^2}{RT} Q_m \left(\frac{\frac{\lambda}{1+\lambda}}{D_{wOH^-}} + \frac{1}{D_{OH^-}(0) \cdot \lambda} \right)^{-1} \tau^{-2}$	c_{OH^-} in mole/liter. Q_m- Molar concentration of fixed positive charges in ionomer	[37]
Degradation rate constant, $k(\lambda, T)$	$k(\lambda, T) = \frac{A}{1+\alpha\lambda}\{1 - tanh[w(\lambda - \lambda_0)]\}e^{-\frac{E_a}{RT}}$	The dependence of the rate constant on the hydration number and temperature	[42]
Degradation kinetics parameters	$A = 3.14 \cdot 10^{17} \frac{1}{s}, \alpha = 5.799, E_a = 1.33 \cdot 10^5 \frac{J}{mole}, w = 6, \lambda_0 = 6$	$A, \alpha, E_a, w, \lambda_0$ are material-specific parameter	[42]
Concentration of hydroxide in the ionomer, c_{OH^-}	$\frac{\partial c_{OH^-}}{\partial t} = -k(\lambda, T) c_{OH^-}$	IEC is denoted by the hydroxide concentration c_{OH^-} (electroneutrality).	[42]

λ_{max}	$\lambda_{max} = \frac{WU(\%)/100}{Mw(H_2O) \cdot IEC}$	Number of waters per cation functional group WU- water uptake Mw (H_2O) = 18.02 g/mol	[60]
Kinetic overpotential, "i" is anode or cathode	$\eta_{kinetic,i} = \frac{1}{I}\int R_{OH^-} \cdot \phi \, dx$	ϕ is electric potential (V) R_{OH^-} is current generation (A m^{-3})	[61][62]

4. Results and discussion

Fig. 1 compares the simulated performance of Pt/C cathode AEMFCs (solid lines) to experimental data (dots) for three AEMs of 5, 20, and 30 μm thickness. The polarization curves shown in Fig. 1a and power density curves shown in Fig. 1b highlight the important effect of membrane thickness on the performance of AEMFCs, with effects beyond what is expected from a pure increase in Ohmic losses, as seen from the shape of the polarization curves and discussed below. While decreasing the AEM thickness from 30 to 20 μm moderately improves cell performance, a further decrease down to 5 μm dramatically enhances it. At 0.6 V, we see a 3-fold increased current density as the AEM thickness is reduced from 30 to 5 μm. This enhancement is the result of a combination of decreased ohmic resistance and enhanced water transport through the membrane. The thinner membrane, associated with a higher gradient of water content between the electrodes, results in higher hydration levels in the membrane and on the cathode side. These high hydration values enhance the hydroxide conductivity (λ-dependent) of the membrane leading to better performance, as discussed in Ref. [31]. Furthermore, the enhanced water transport from anode to cathode with a thin membrane provides sufficient water to participate in the electrochemical reaction (especially

the ORR) and thus reduces the activation losses. For example, at 0.8 V, a 5-times higher current density, from 0.1 to 0.5 A cm^{-2}, is observed when membrane thickness is reduced from 30 to 5 µm.

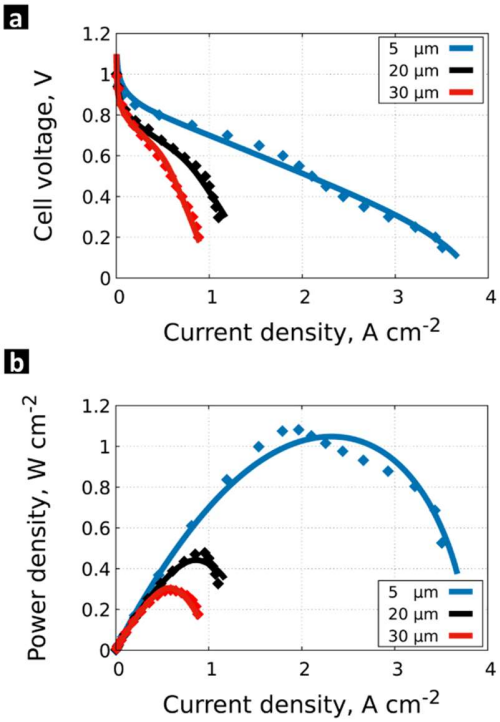

Fig. 1. *Comparison of simulated (solid curves) and experimental (dots) (a) initial polarization curves and (b) power density curves of AEMFCs with Pt/C cathode made with AEMs with different thickness of 5, 20, and 30 µm. The cell temperature was 60 °C, RH anode and cathode = 100 %, without backpressure. The anode and cathode catalyst loadings were 0.70* mg_{PtRu} cm^{-2} *and 0.70* mg_{Pt} cm^{-2}*, respectively.*

Next, our AEMFC model [42] is used to simulate initial polarization curves in order to quantify the effect of membrane thickness on cell performance and increase the understanding of water management through the cell. Firstly, the model is validated against experimental data for AEMFC with a membrane thickness of 30 µm by tuning a single parameter for fitting the entire dataset,

namely, the cathode electrochemical surface area. The remaining model parameters, shown in Tables 1 and 2, were derived from literature review, technical data sheets (from Fumatech), and experimental measurements [54,57,63,64]. Then, for validating all other AEMFC performance curves, the only parameter to update was AEM thickness. Fig. 1a depicts a good agreement between the simulated and experimental cell performances for all AEMs, over a broad range of current densities (from 0 to 3.5 A cm^{-2}). The good agreement between model predictions and experimental data obtained after tuning only the electrochemical surface area provides strong confidence in the model validity and robustness.

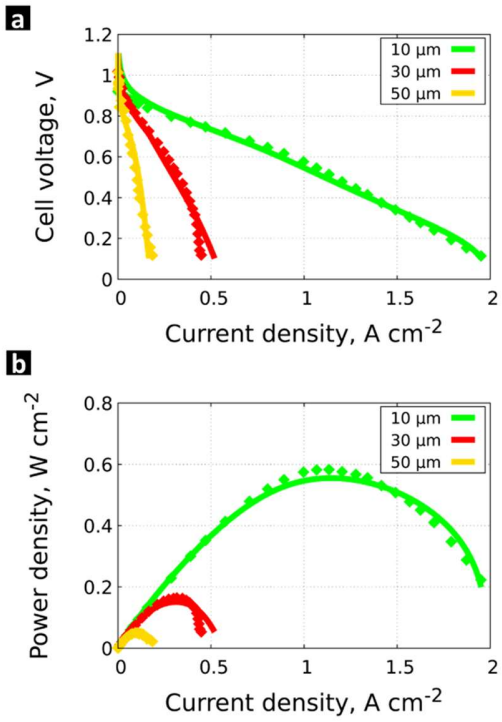

Fig. 2. *Comparison of simulated (solid curves) and experimental (dots) (a) initial polarization curves and (b) power density curves of AEMFCs with Fe-N-C cathode made with AEMs with different thickness of 10, 30, and 50 µm. The cell temperature was 60 °C with 83 % RH at anode*

and 94 % RH at the cathode. Anode backpressure is zero while cathode backpressure is 2 bar. The anode and cathode catalyst loadings were 0.4 mg_{PtRu} cm^{-2} and 0.8 $mg_{Fe\text{-}N\text{-}C}$ cm^{-2}, respectively.

To further explore the effect of AEM thickness on cell performance, we tested additional AEMFCs with different MEAs and operating conditions. Fig. 2a shows experimental polarization curves of AEMFCs, with the dataset obtained using the Fe-N-C cathode, for different AEM thickness values (10, 30, and 50 μm). Similar to the case of Pt/C cathode, Fig. 2a shows a significant improvement in cell performance as AEM thickness decreases while, as in Fig. 1b, the Fig. 2b shows the effect on the power density curves. For example, at 0.6 and 0.8 V, we see an 8.5-fold increased current density, from 0.1 to 0.85 A cm^{-2} and from 0.04 to 0.34 A cm^{-2}, respectively, as the AEM thickness is reduced from 50 to 10 μm. However, when compared to the results obtained using the Pt/C cathode, the overall cell performance is lower. For instance, for the AEMFC made with the 30 μm AEM, we see a nearly 50 % reduction in limiting current density (at 0.2 V). Nevertheless, at 0.8 V, both cells with Pt/C and Fe-N-C cathode exhibit a similar current density of 0.1 A cm^{-2}. This is mainly due to the different character of catalysts used in the cathodes, as well as the different anode catalyst loadings and operating conditions used in the Fe-N-C-based cells. Figs. 1 and 2 show that, despite using different cathode catalysts and operating conditions in the AEMFCs, membrane thickness remains a critical factor in determining the whole cell performance.

We then simulate the initial polarization curves of the cells with the Fe-N-C cathode and various AEM thickness values (10, 30, and 50 μm). Similar to the results in Fig. 1, using the cathode electrochemical surface area as a single fitting parameter, model validation is achieved against the AEMFC with a membrane thickness of 50 μm. The thicknesses of the different AEMs were then updated without additional fitting parameters. The simulated initial performance of all three cells, displayed in Fig. 2, agrees excellently with the experimental polarization curves. These validations

further assure the model's confidence and accuracy for analysis and understanding of AEMFCs behavior.

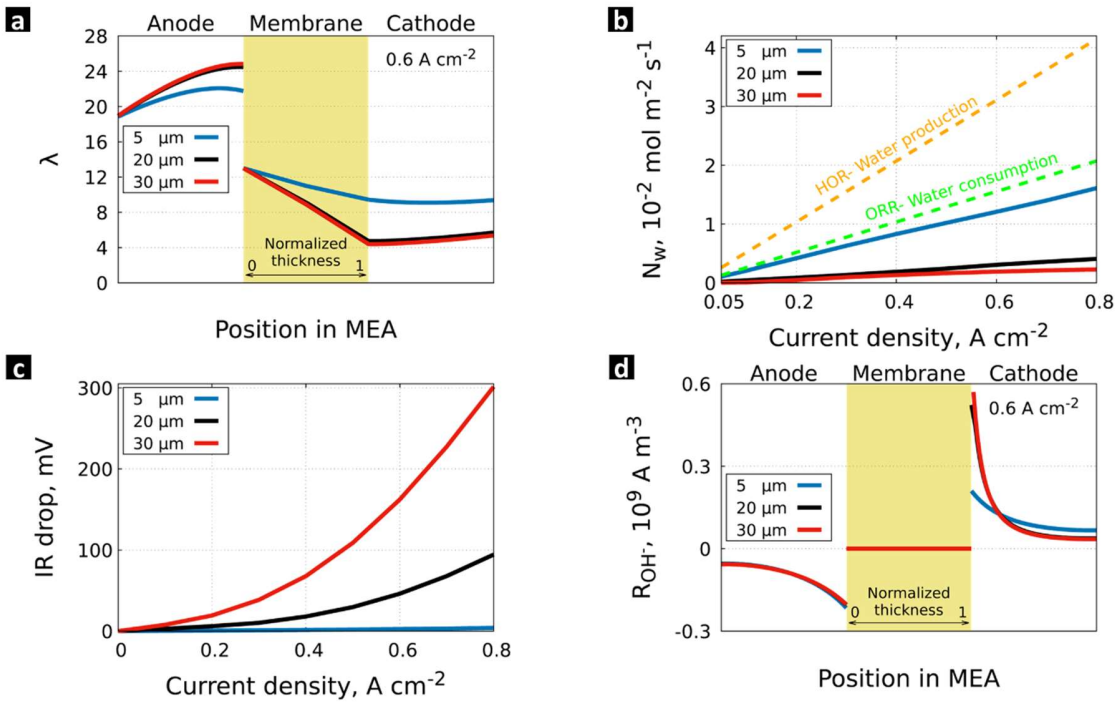

Fig. 3. *(a) Simulated λ profiles at a constant current density of 0.6 A cm^{-2}, (b) diffusive water flux through the membrane, from the anode to the cathode as well as water consumption/production rates, (c) IR (ohmic) drop as a function of current density, and (d) reaction distribution profiles at a constant current density of 0.6 A cm^{-2}. Note that the membrane thickness is normalized; anode and cathode CL thickness is 60 μm.*

In Fig. 3, we analyze the effect of membrane thickness on cell performance for the case of AEMFCs with the Pt/C cathode (Fig. 1a). First, Fig. 3a shows hydration levels (λ = number of water molecules per hydroxide ion) across the cell for an AEMFC operated at a current density of 0.6 A cm^{-2}. The results show a significant reduction in the difference in hydration number values between the electrodes as the membrane thickness decreases from 30 to 5 μm; this is a direct result

of an *increase* (with decreasing membrane thickness) in the *dimensional* gradient of λ across the membrane[1]. The thin membrane thus results in more efficient water removal from the anode (lower λ), and supplies more water to the cathode side via diffusion, leading to increased λ values from 4.5 to 9, at the membrane-cathode interface, for a membrane thickness of 30 and 5 μm, respectively. The high hydration of the membrane, in turn, enhances the anionic conductivity of the ionomeric materials.

Next, in Fig. 3b we show the calculated water flux through the membrane, from the anode to the cathode (positive flux) as well as the consumption/production of water due to electrochemical reactions. The water flux for the three cells with Pt/C cathode (i.e., with AEMs of 5, 20, and 30 μm) is lower than the water consumption needed for the ORR at this current density, indicating that additional water must be supplied at the cathode through the gas phase from the cathode gas feed. Comparing the three cases, a reduced membrane thickness leads to an increase of the water flux through the membrane towards the cathode, resulting in higher cathode hydration levels, as depicted in Fig. 3a. On the other hand, as membrane thickness increases, the value of the water flux becomes very small compared to the rate of water production due to the HOR. This can quickly lead to anode flooding if additional water removal via the gas phase from the anode is not fast enough. Therefore, with a thinner AEM allowing higher water flux, the water balance is generally easier and the cell can be operated under higher current densities without anode flooding and cathode dry-out issues.

Next, in Fig. 3c, the IR (ohmic) drop is calculated as a function of current density, up to 0.8 A cm-

[1] Notice that the *dimensionless* gradient in λ appears (in Fig. 3) to decrease as membrane thickness is decreased. However, the *dimensional* gradient (which is proportional to the flux of water) actually increases with decreasing membrane thickness.

^{2}, for the three different membrane thickness values. Fig. 3c indeed shows that the performance decay, depicted in Fig. 1a, can be attributed to voltage loss due to the membrane. The results show that the nonlinear nature of IR curves reflects the dependence of membrane resistance on current density. Decreasing membrane thickness, which is associated with enhanced water (Figs. 3a,b) and hydroxide transport, significantly minimizes the ohmic drop across the membrane. For instance, at a current density of 0.6 A cm^{-2}, the IR drop with a membrane thickness of 30 μm contributes to around 160 mV of the total voltage loss, while a negligible IR drop is observed with the 5 μm membrane.

Finally, Fig. 3d demonstrates the local reaction rate across the anode and cathode CLs for the three cells, at a given current density of 0.6 A cm^{-2}. Besides the apparent effect of membrane thickness on the voltage losses due to transport through the membrane shown in Fig. 3c, it also has a substantial impact on the reaction distribution through the cathode CL. Thanks to the higher hydration levels in the cathode as membrane thickness decreases, a more uniform reaction distribution is observed in the cathode CL with the 5 μm AEM, indicating a better catalyst utilization. With thicker membranes (20 and 30 μm), however, the reaction is concentrated at the membrane-cathode CL interface, due to low water supply from the anode to the cathode, as can be seen in Fig. 3d. This implies a higher overpotential to drive the ORR (lower cathode performance). Overall, the combined experimental and model results show that the effect of AEM thickness in AEMFC is complex, going well beyond the sole proportional increase of IR drop with thickness. The AEM thickness deeply changes the water balance, modifying the gradient of ionic conductivity throughout the entire AEM (modifying therefore the IR drop in a non-proportional way with AEM thickness), but also through the cathode CL, impacting the catalyst utilization and cathode performance as well.

The effect of membrane thickness on the hydration levels is further studied and clarified in Fig. 4a. The calculated λ values at the membrane-cathode interface are plotted as iso-λ curves in a 2D color map, as a function of the AEM thickness and operating current density. From Fig. 4a it is evident that decreasing membrane thickness, for a constant current density, enhances the hydration level at the membrane-cathode interface. These enhanced hydration levels at the cathode CL also favor the AEMFC performance stability, as we previously described in [31,42,43]. The calculated degradation rate as a function of lambda value is indicated on the bar graph in Fig.4, showing an increase by several orders of magnitude of the degradation rate at the AEM-cathode interface when cathode dry-out takes place. In line with this, a recent experimental study with a Fe-N-C cathode suggests that the cell performance loss observed after 100 h operation takes place at the cathode CL, but leads essentially to ionomer degradation with little impact on the ORR activity of Fe-N-C [5]. Finally, the enhanced hydration levels shown in Fig. 4a cause an increase in the hydroxide conductivity in the membrane, increasing in turn the cell performance. Fig. 4b shows the local hydroxide conductivity simulated in the membrane-cathode interface. Figs. 4a,b show the relative relationship between the current density and the AEM thickness to achieve the same degrees of hydration and hydroxide conductivity at the membrane-cathode interface, gaining further understanding of the influence of membrane thickness on the water management in AEMFCs.

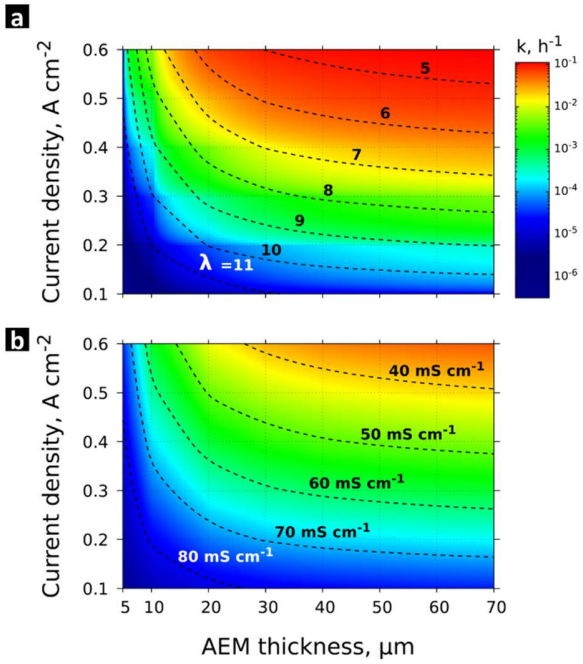

Fig. 4. *2D contour plot (colormap) and AEMFC with Pt/C cathode operating curves (dash lines) of (a) hydration levels at the membrane/ cathode and ionomeric material degradation rate constant k; and (b) hydroxide conductivity at the membrane/cathode interface, as a function of membrane thickness and operating current density* [43].

5. Conclusion

The anion-exchange membrane thickness is a critical parameter affecting the performance and stability of AEMFCs. In this study, we investigated experimentally and theoretically the effect of membrane thickness on AEMFC performance using both PGM-based and PGM-free cathode catalysts. Furthermore, we provide a comprehensive analysis of the performance of the PGM-based cathode catalyst using a 1D model of AEMFC. The high level of adequacy agreement between the experimental results and model predictions emphasizes the validity and robustness of our AEMFC model. The results show a significant enhancement in cell performance with the

reduction of AEM thickness. This is mainly due to the enhanced water transport from the anode, through the AEM, towards the cathode electrode. Furthermore, thin AEM reduces the likelihood of anode flooding, increases local hydration in the membrane, and provides enough water to the cathode CL, resulting in higher hydration levels. As a result, the conductivity of the ionomeric material both in the membrane and in the cathode is enhanced. Overall, the quantitative and qualitative modeling results adequately explain water management in AEMFCs, demonstrating the importance of using thinner AEM for better water management in AEMFCs, ultimately leading to higher cell performance.

6. Declaration of Competing Interest

The authors declare that they have no known competing financial interests or personal relationships that could have appeared to influence the work reported in this paper.

7. Acknowledgments

This work was partially funded by the Nancy & Stephen Grand Technion Energy Program (GTEP); the European Union's Horizon 2020 research and innovation programme under grant agreement CREATE [721065], the French-Israeli Joint Research Project (PRC 2019–2021; MOST and CNRS) [PRC2347] (MOST grant No.3-15578); the Ministry of National Infrastructure, Energy and Water Resources of Israel through grant No. 3-16686 (219-11-135), the Mauerberger Foundation Fund (MFF); and the Israel Science Foundation through grant No. 1934/17. KY would also like to acknowledge the financial support of the Zvi Yanai fellowship of the Ministry of Science and technology. The authors would like to thank Dr. Michael Schuster

and Dr. Bernd Bauer from Fumatech GmbH (Germany) for their generous supply of the membranes for this study.

References

[1] D.R. Dekel, Review of cell performance in anion exchange membrane fuel cells, J. Power Sources. 375 (2018) 158–169. https://doi.org/10.1016/j.jpowsour.2017.07.117.

[2] S. Gottesfeld, D.R. Dekel, M. Page, C. Bae, Y. Yan, P. Zelenay, Y.S. Kim, Anion exchange membrane fuel cells: Current status and remaining challenges, J. Power Sources. 375 (2018) 170–184. https://doi.org/10.1016/j.jpowsour.2017.08.010.

[3] T.B. Ferriday, P.H. Middleton, Alkaline fuel cell technology - A review, Int. J. Hydrogen Energy. 46 (2021) 18489–18510. https://doi.org/10.1016/j.ijhydene.2021.02.203.

[4] J.C. Douglin, R.K. Singh, S. Haj, S. Li, J. Biemolt, N. Yan, J.R. Varcoe, G. Rothenberg, D. Dekel, A High-Temperature Anion-Exchange Membrane Fuel Cell with a Critical Raw Material-free Cathode, Chem. Eng. J. Adv. 8 (2021) 100153. https://doi.org/10.1016/j.ceja.2021.100153.

[5] H. Adabi, P. Giovanni, A. Shakouri, X. Peng, K. Yassin, I.G. Rasin, S. Brandon, D.R. Dekel, N. Ul, M. Sougrati, A. Zitolo, J.R. Varcoe, J.R. Regalbuto, Understanding how single-atom site density drives the performance and durability of PGM-free Fe e N e C cathodes in anion exchange membrane fuel cells d e, 12 (2021). https://doi.org/10.1016/j.mtadv.2021.100179.

[6] D. Pinsky, N. Ralbag, R.K. Singh, M. Mann-Lahav, G.E. Shter, D.R. Dekel, G.S. Grader,

D. Avnir, Metal nanoparticles entrapped in metal matrices, Nanoscale Adv. (2021). https://doi.org/10.1039/d1na00315a.

[7] J. Biemolt, J.C. Douglin, R.K. Singh, E.S. Davydova, N. Yan, G. Rothenberg, D.R. Dekel, An Anion-Exchange Membrane Fuel Cell Containing Only Abundant and Affordable Materials, Energy Technol. 9 (2021) 5–9. https://doi.org/10.1002/ente.202000909.

[8] V.M. Truong, J.R. Tolchard, J. Svendby, M. Manikandan, H.A. Miller, S. Sunde, H. Yang, D.R. Dekel, A.O. Barnett, Platinum and platinum group metal-free catalysts for anion exchange membrane fuel cells, Energies. 13 (2020) 1–21. https://doi.org/10.3390/en13030582.

[9] E. Negro, A. Bach Delpeuch, K. Vezzù, G. Nawn, F. Bertasi, A. Ansaldo, V. Pellegrini, B. Dembinska, S. Zoladek, K. Miecznikowski, I.A. Rutkowska, M. Skunik-Nuckowska, P.J. Kulesza, F. Bonaccorso, V. Di Noto, Toward Pt-Free Anion-Exchange Membrane Fuel Cells: Fe-Sn Carbon Nitride-Graphene Core-Shell Electrocatalysts for the Oxygen Reduction Reaction, Chem. Mater. 30 (2018) 2651–2659. https://doi.org/10.1021/acs.chemmater.7b05323.

[10] P.G. Santori, F.D. Speck, S. Cherevko, H.A. Firouzjaie, X. Peng, W.E. Mustain, F. Jaouen, High Performance FeNC and Mn-oxide/FeNC Layers for AEMFC Cathodes, J. Electrochem. Soc. 167 (2020) 134505. https://doi.org/10.1149/1945-7111/abb7e0.

[11] J. Lilloja, E. Kibena-Põldsepp, A. Sarapuu, A. Kikas, V. Kisand, M. Käärik, M. Merisalu, A. Treshchalov, J. Leis, V. Sammelselg, Q. Wei, S. Holdcroft, K. Tammeveski, Nitrogen-doped carbide-derived carbon/carbon nanotube composites as cathode catalysts for anion

exchange membrane fuel cell application, Appl. Catal. B Environ. 272 (2020) 119012. https://doi.org/10.1016/j.apcatb.2020.119012.

[12] Y. Xue, L. Shi, X. Liu, J. Fang, X. Wang, B.P. Setzler, W. Zhu, Y. Yan, Z. Zhuang, A highly-active, stable and low-cost platinum-free anode catalyst based on RuNi for hydroxide exchange membrane fuel cells, Nat. Commun. 11 (2020) 1–8. https://doi.org/10.1038/s41467-020-19413-5.

[13] A. Sokka, M. Mooste, M. Käärik, V. Gudkova, J. Kozlova, A. Kikas, V. Kisand, A. Treshchalov, A. Tamm, P. Paiste, J. Aruväli, J. Leis, A. Krumme, S. Holdcroft, S. Cavaliere, F. Jaouen, K. Tammeveski, Iron and cobalt containing electrospun carbon nanofibre-based cathode catalysts for anion exchange membrane fuel cell, Int. J. Hydrogen Energy. 46 (2021) 31275–31287. https://doi.org/10.1016/j.ijhydene.2021.07.025.

[14] A. Roy, M.R. Talarposhti, S.J. Normile, I. V. Zenyuk, V. De Andrade, K. Artyushkova, A. Serov, P. Atanassov, Nickel-copper supported on a carbon black hydrogen oxidation catalyst integrated into an anion-exchange membrane fuel cell, Sustain. Energy Fuels. 2 (2018) 2268–2275. https://doi.org/10.1039/c8se00261d.

[15] N. Zion, J.C. Douglin, D.A. Cullen, P. Zelenay, D.R. Dekel, L. Elbaz, Porphyrin Aerogel Catalysts for Oxygen Reduction Reaction in Anion-Exchange Membrane Fuel Cells, Adv. Funct. Mater. 2100963 (2021) 2100963. https://doi.org/10.1002/adfm.202100963.

[16] W. Zhu, Y. Pei, J.C. Douglin, J. Zhang, H. Zhao, J. Xue, Q. Wang, R. Li, Y. Qin, Y. Yin, D.R. Dekel, M.D. Guiver, Multi-scale study on bifunctional Co/Fe–N–C cathode catalyst

layers with high active site density for the oxygen reduction reaction, Appl. Catal. B Environ. 299 (2021) 120656. https://doi.org/10.1016/j.apcatb.2021.120656.

[17] M. Hren, M. Božič, D. Fakin, K.S. Kleinschek, S. Gorgieva, Alkaline membrane fuel cells: Anion exchange membranes and fuels, Sustain. Energy Fuels. 5 (2021) 604–637. https://doi.org/10.1039/d0se01373k.

[18] A.L.G. Biancolli, S. Bsoul-Haj, J.C. Douglin, A.S. Barbosa, R.R. de Sousa, O. Rodrigues, A.J.C. Lanfredi, D.R. Dekel, E.I. Santiago, High-performance radiation grafted anion-exchange membranes for fuel cell applications: Effects of irradiation conditions on ETFE-based membranes properties, J. Memb. Sci. 641 (2022). https://doi.org/10.1016/j.memsci.2021.119879.

[19] S. Maurya, S. Noh, I. Matanovic, E.J. Park, C. Narvaez Villarrubia, U. Martinez, J. Han, C. Bae, Y.S. Kim, Rational design of polyaromatic ionomers for alkaline membrane fuel cells with >1 W cm-2 power density, Energy Environ. Sci. 11 (2018) 3283–3291. https://doi.org/10.1039/c8ee02192a.

[20] J. Wang, Y. Zhao, B.P. Setzler, S. Rojas-Carbonell, C. Ben Yehuda, A. Amel, M. Page, L. Wang, K. Hu, L. Shi, S. Gottesfeld, B. Xu, Y. Yan, Poly(aryl piperidinium) membranes and ionomers for hydroxide exchange membrane fuel cells, Nat. Energy. 4 (2019) 392–398. https://doi.org/10.1038/s41560-019-0372-8.

[21] M. Kumari, J.C. Douglin, D.R. Dekel, Crosslinked quaternary phosphonium-functionalized poly(ether ether ketone) polymer-based anion-exchange membranes, J. Memb. Sci. 626 (2021) 119167. https://doi.org/10.1016/j.memsci.2021.119167.

[22] P. Veh, B. Britton, S. Holdcroft, R. Zengerle, S. Vierrath, M. Breitwieser, Improving the water management in anion-exchange membrane fuel cells: via ultra-thin, directly deposited solid polymer electrolyte, RSC Adv. 10 (2020) 8645–8652. https://doi.org/10.1039/c9ra09628k.

[23] A. Allushi, T.H. Pham, P. Jannasch, Highly conductive hydroxide exchange membranes containing fluorene-units tethered with dual pairs of quaternary piperidinium cations, J. Memb. Sci. 632 (2021) 119376. https://doi.org/10.1016/j.memsci.2021.119376.

[24] J. Fan, S. Willdorf-Cohen, E.M. Schibli, Z. Paula, W. Li, T.J.G. Skalski, A.T. Sergeenko, A. Hohenadel, B.J. Frisken, E. Magliocca, W.E. Mustain, C.E. Diesendruck, D.R. Dekel, S. Holdcroft, Poly(bis-arylimidazoliums) possessing high hydroxide ion exchange capacity and high alkaline stability, Nat. Commun. 10 (2019). https://doi.org/10.1038/s41467-019-10292-z.

[25] L. Wang, X. Peng, W.E. Mustain, J.R. Varcoe, Radiation-grafted anion-exchange membranes: the switch from low- to high-density polyethylene leads to remarkably enhanced fuel cell performance, Energy Environ. Sci. (2019) 1575–1579. https://doi.org/10.1039/C9EE00331B.

[26] T. Huang, G. He, J. Xue, O. Otoo, X. He, H. Jiang, J. Zhang, Y. Yin, Z. Jiang, J.C. Douglin, D.R. Dekel, M.D. Guiver, Self-crosslinked blend alkaline anion exchange membranes with bi-continuous phase separated morphology to enhance ion conductivity, J. Memb. Sci. 597 (2020) 117769. https://doi.org/10.1016/j.memsci.2019.117769.

[27] M. Mandal, G. Huang, N.U. Hassan, W.E. Mustain, P.A. Kohl, Poly(norbornene) anion

conductive membranes: homopolymer, block copolymer and random copolymer properties and performance, J. Mater. Chem. A. 8 (2020) 17568–17578. https://doi.org/10.1039/d0ta04756b.

[28] T.J. Omasta, A.M. Park, J.M. LaManna, Y. Zhang, X. Peng, L. Wang, D.L. Jacobson, J.R. Varcoe, D.S. Hussey, B.S. Pivovar, W.E. Mustain, Beyond catalysis and membranes: visualizing and solving the challenge of electrode water accumulation and flooding in AEMFCs, Energy Environ. Sci. 11 (2018) 551–558. https://doi.org/10.1039/C8EE00122G.

[29] T.J. Omasta, A.M. Park, J.M. Lamanna, Y. Zhang, X. Peng, L. Wang, D.L. Jacobson, J.R. Varcoe, D.S. Hussey, B.S. Pivovar, W.E. Mustain, Beyond catalysis and membranes: Visualizing and solving the challenge of electrode water accumulation and flooding in AEMFCs, Energy Environ. Sci. 11 (2018) 551–558. https://doi.org/10.1039/c8ee00122g.

[30] T.J. Omasta, L. Wang, X. Peng, C.A. Lewis, J.R. Varcoe, W.E. Mustain, Importance of balancing membrane and electrode water in anion exchange membrane fuel cells, J. Power Sources. 375 (2018) 205–213. https://doi.org/10.1016/j.jpowsour.2017.05.006.

[31] K. Yassin, I.G. Rasin, S. Brandon, D.R. Dekel, Quantifying the critical effect of water diffusivity in anion exchange membranes for fuel cell applications, J. Memb. Sci. (2020). https://doi.org/10.1016/j.memsci.2020.118206.

[32] M.R. Gerhardt, L.M. Pant, A.Z. Weber, Along-the-Channel Impacts of Water Management and Carbon-Dioxide Contamination in Hydroxide-Exchange-Membrane Fuel Cells: A Modeling Study, J. Electrochem. Soc. 166 (2019) F3180–F3192.

https://doi.org/10.1149/2.0171907jes.

[33] D.P. Leonard, S. Maurya, E.J. Park, L. Delfin Manriquez, S. Noh, X. Wang, C. Bae, E.D. Baca, C. Fujimoto, Y.S. Kim, Asymmetric electrode ionomer for low relative humidity operation of anion exchange membrane fuel cells, J. Mater. Chem. A. 8 (2020) 14135–14144. https://doi.org/10.1039/d0ta05807f.

[34] B. Eriksson, H. Grimler, A. Carlson, H. Ekström, R. Wreland Lindström, G. Lindbergh, C. Lagergren, Quantifying water transport in anion exchange membrane fuel cells, Int. J. Hydrogen Energy. 44 (2019) 4930–4939. https://doi.org/10.1016/j.ijhydene.2018.12.185.

[35] R. Gutru, Z. Turtayeva, F. Xu, G. Maranzana, B. Vigolo, A. Desforges, A comprehensive review on water management strategies and developments in anion exchange membrane fuel cells, Int. J. Hydrogen Energy. 45 (2020) 19642–19663. https://doi.org/10.1016/j.ijhydene.2020.05.026.

[36] J. Zhang, Y. Liu, W. Zhu, Y. Pei, Y. Yin, Y. Qin, X. Li, M.D. Guiver, Self-adjusting anode catalyst layer for smart water management in anion exchange membrane fuel cells, Cell Reports Phys. Sci. 2 (2021) 100377. https://doi.org/10.1016/j.xcrp.2021.100377.

[37] D.R. Dekel, I.G. Rasin, M. Page, S. Brandon, Steady state and transient simulation of anion exchange membrane fuel cells, J. Power Sources. 375 (2018) 191–204. https://doi.org/10.1016/j.jpowsour.2017.07.012.

[38] M. Mandal, G. Huang, N.U. Hassan, X. Peng, T. Gu, A.H. Brooks-Starks, B. Bahar, W.E. Mustain, P.A. Kohl, The Importance of Water Transport in High Conductivity and High-Power Alkaline Fuel Cells, J. Electrochem. Soc. 167 (2020) 054501.

https://doi.org/10.1149/2.0022005jes.

[39] L. Wang, M. Bellini, H.A. Miller, J.R. Varcoe, A high conductivity ultrathin anion-exchange membrane with 500+ h alkali stability for use in alkaline membrane fuel cells that can achieve 2 W cm−2 at 80 °C, J. Mater. Chem. A. 6 (2018) 15404–15412. https://doi.org/10.1039/c8ta04783a.

[40] D. Saebea, C. Chaiburi, S. Authayanun, Model based evaluation of alkaline anion exchange membrane fuel cells with water management, Chem. Eng. J. 374 (2019) 721–729. https://doi.org/10.1016/j.cej.2019.05.200.

[41] Y. Oshiba, J. Hiura, Y. Suzuki, T. Yamaguchi, Improvement in the solid-state alkaline fuel cell performance through efficient water management strategies, J. Power Sources. 345 (2017) 221–226. https://doi.org/10.1016/j.jpowsour.2017.01.111.

[42] D.R. Dekel, I.G. Rasin, S. Brandon, Predicting performance stability of anion exchange membrane fuel cells, J. Power Sources. 420 (2019) 118–123. https://doi.org/10.1016/j.jpowsour.2019.02.069.

[43] K. Yassin, I.G. Rasin, S. Willdorf-cohen, C.E. Diesendruck, S. Brandon, D.R. Dekel, A surprising relation between operating temperature and stability of anion exchange membrane fuel cells, J. Power Sources Adv. 11 (2021) 100066. https://doi.org/10.1016/j.powera.2021.100066.

[44] H. Deng, D. Wang, X. Xie, Y. Zhou, Y. Yin, Q. Du, K. Jiao, Modeling of hydrogen alkaline membrane fuel cell with interfacial effect and water management optimization, Renew. Energy. 91 (2016) 166–177. https://doi.org/10.1016/j.renene.2016.01.054.

[45] S. Huo, J.W. Park, P. He, D. Wang, K. Jiao, Analytical modeling of liquid saturation jump effect for hydrogen alkaline anion exchange membrane fuel cell, Int. J. Heat Mass Transf. 112 (2017) 891–902. https://doi.org/10.1016/j.ijheatmasstransfer.2017.04.137.

[46] S. Huo, J. Zhou, T. Wang, R. Chen, K. Jiao, Experimental and analytical analysis of polarization and water transport behaviors of hydrogen alkaline membrane fuel cell, J. Power Sources. 382 (2018) 1–12. https://doi.org/10.1016/j.jpowsour.2018.02.020.

[47] B.S. Machado, M. Mamlouk, N. Chakraborty, Three-dimensional agglomerate model of an anion exchange membrane fuel cell using air at the cathode – A parametric study, J. Power Sources. 412 (2019) 105–117. https://doi.org/10.1016/j.jpowsour.2018.11.022.

[48] W.Q. Tao, C.H. Min, X.L. Liu, Y.L. He, B.H. Yin, W. Jiang, Parameter sensitivity examination and discussion of PEM fuel cell simulation model validation. Part I. Current status of modeling research and model development, J. Power Sources. 160 (2006) 359–373. https://doi.org/10.1016/j.jpowsour.2006.01.078.

[49] A. Zitolo, V. Goellner, V. Armel, M.T. Sougrati, T. Mineva, L. Stievano, E. Fonda, F. Jaouen, Identification of catalytic sites for oxygen reduction in iron- and nitrogen-doped graphene materials, Nat. Mater. 14 (2015) 937–942. https://doi.org/10.1038/nmat4367.

[50] J.C. Douglin, J.R. Varcoe, D.R. Dekel, A high-temperature anion-exchange membrane fuel cell, J. Power Sources Adv. 5 (2020) 100023. https://doi.org/10.1016/j.powera.2020.100023.

[51] S. Wierzbicki, J.C. Douglin, A. Kostuch, D.R. Dekel, K. Kruczala, Are radicals formed during anion-exchange membrane fuel cell operation?, J. Phys. Chem. Lett. 11 (2020)

7630–7636. https://doi.org/https://doi.org/10.1021/acs.jpclett.0c02349.

[52] T.J. Omasta, X. Peng, H.A. Miller, F. Vizza, L. Wang, J.R. Varcoe, D.R. Dekel, W.E. Mustain, Beyond 1.0 W cm −2 Performance without Platinum: The Beginning of a New Era in Anion Exchange Membrane Fuel Cells , J. Electrochem. Soc. 165 (2018) J3039–J3044. https://doi.org/10.1149/2.0071815jes.

[53] A. Zhegur-Khais, F. Kubannek, U. Krewer, D.R. Dekel, Measuring the true hydroxide conductivity of anion exchange membranes, J. Memb. Sci. 612 (2020) 118461. https://doi.org/10.1016/j.memsci.2020.118461.

[54] M.G. Marino, J.P. Melchior, A. Wohlfarth, K.D. Kreuer, Hydroxide, halide and water transport in a model anion exchange membrane, J. Memb. Sci. 464 (2014) 61–71. https://doi.org/10.1016/j.memsci.2014.04.003.

[55] J.P. Melchior, W. Lohstroh, M. Zamponi, N.H. Jalarvo, Multiscale water dynamics in model Anion Exchange Membranes for Alkaline Membrane Fuel Cells, J. Memb. Sci. 586 (2019) 240–247. https://doi.org/10.1016/j.memsci.2019.05.079.

[56] J.P. Melchior, N.H. Jalarvo, A Quasielastic Neutron Scattering Study of Water Diffusion in Model Anion Exchange Membranes over Localized and Extended Volume Increments, J. Phys. Chem. C. 123 (2019) 14195–14206. https://doi.org/10.1021/acs.jpcc.9b01873.

[57] P. Fortin, T. Khoza, X. Cao, S.Y. Martinsen, A. Oyarce Barnett, S. Holdcroft, High-performance alkaline water electrolysis using Aemion^{TM} anion exchange membranes, J. Power Sources. 451 (2020) 227814. https://doi.org/10.1016/j.jpowsour.2020.227814.

[58] Z. Noga, A.N. Mondal, T. Weissbach, H. Steven, D.R. Dekel, Effect of of CO2 on the properties of anion exchange membranes for fuel cell applications, Macromolecules. 586 (2019) 140–150. https://doi.org/10.1016/j.memsci.2019.05.053.

[59] T. Zelovich, L. Vogt-Maranto, C. Simari, I. Nicotera, M.A. Hickner, S.J. Paddison, C. Bae, D.R. Dekel, M.E. Tuckerman, Non-Monotonic Temperature Dependence of Hydroxide Ion Diffusion in Anion Exchange Membranes, Chem. Mater. (2022). https://doi.org/10.1021/acs.chemmater.1c03594.

[60] M.A. Vandiver, B.R. Caire, J.R. Carver, K. Waldrop, M.R. Hibbs, J.R. Varcoe, A.M. Herring, M.W. Liberatore, Mechanical Characterization of Anion Exchange Membranes by Extensional Rheology under Controlled Hydration, J. Electrochem. Soc. 161 (2014) H677–H683. https://doi.org/10.1149/2.0971410jes.

[61] K. Yassin, I.G. Rasin, S. Brandon, D.R. Dekel, Elucidating the role of anion-exchange ionomer conductivity within the cathode catalytic layer of anion-exchange membrane fuel cells, J. Power Sources. 524 (2022) 231083. https://doi.org/10.1016/j.jpowsour.2022.231083.

[62] J. Newman, K.E. Thomas-Alyea, Electrochemical systems, John Wiley & Sons, 2004.

[63] D. Ion-Ebrasu, B.G. Pollet, S. Caprarescu, A. Chitu, R. Trusca, V. Niculescu, R. Gabor, E. Carcadea, M. Varlam, B.S. Vasile, Graphene inclusion effect on anion-exchange membranes properties for alkaline water electrolyzers, Int. J. Hydrogen Energy. 45 (2020) 17057–17066. https://doi.org/10.1016/j.ijhydene.2020.04.195.

[64] Q. Li, H. Peng, Y. Wang, L. Xiao, J. Lu, L. Zhuang, The Comparability of Pt to Pt-Ru in

Catalyzing the Hydrogen Oxidation Reaction for Alkaline Polymer Electrolyte Fuel Cells Operated at 80 °C, Angew. Chemie - Int. Ed. 58 (2019) 1442–1446. https://doi.org/10.1002/anie.201812662.